

# InSAR measured permafrost degradation of palsa peatlands in northern Sweden

**Authors:** Samuel Valman<sup>1,2\*</sup>, Matthias B. Siewert<sup>3\*</sup>, Doreen Boyd<sup>2</sup>, Martha Ledger<sup>4,5</sup>, David Gee<sup>6</sup>, Betsabe de la Barreda-Bautista<sup>4,2</sup>, Andrew Sowter<sup>6</sup>, Sofie Sjogersten<sup>4</sup>

## Affiliations:

<sup>1</sup> Nottingham Geospatial Institute, University of Nottingham, Nottingham NG7 2TU, UK

<sup>2</sup> School of Geography, University of Nottingham, University Park, NG7 2RD, Nottingham, UK

<sup>3</sup> Department of Ecology and Environmental Sciences, Umeå University, Umeå, Sweden

<sup>4</sup> School of Biosciences, University of Nottingham, Sutton Bonington Campus, College Road, LE12 5RD, Loughborough, UK

<sup>5</sup> School of Biological Sciences, Kadoorie Biological Sciences Building, University of Hong Kong, Pok Fu Lam Road, Hong Kong

<sup>6</sup> TerraMotion, Ingenuity Centre, Triumph Rd, Nottingham NG7 2TU

\*These authors contributed equally to this work.

Corresponding author: Sofie Sjogersten [sofie.sjogersten@nottingham.ac.uk](mailto:sofie.sjogersten@nottingham.ac.uk)

**Abstract.** Climate warming is degrading palsa peatlands across the circumpolar permafrost region. Permafrost degradation may lead to ecosystem collapse and potentially strong climate feedbacks, as this ecosystem is an important carbon store and can transition to being a strong methane emitter. Landscape level measurement of permafrost degradation is needed to monitor this impact of warming. Surface subsidence is a useful metric of change and can be monitored using InSAR satellite technology. We combined InSAR data, processed using the ASPIS algorithm to monitor ground motion between 2017 and 2021, with airborne optical and LiDAR data to investigate the rate of subsidence across palsa peatlands in northern Sweden. We show that 55% of Sweden's eight largest palsa peatlands are currently subsiding, which can be attributed to these permafrost landforms and their degradation. The most rapid degradation occurring in the largest palsa complexes in the most northern part of the region of study, also corresponding to the areas with the highest % palsa cover within the overall mapped wetland area. Further, higher degradation rates were found in areas where winter precipitation has increased substantially. The roughness index calculated from a LiDAR-derived DEM, used as a proxy for degradation, increases alongside subsidence rates and may be used as a complementary proxy for palsa degradation. We show that combining datasets captured using remote sensing enables regional-scale estimation of ongoing permafrost degradation, an important step towards estimating the future impact of climate change on permafrost-dependent ecosystems.

**Keywords:** Permafrost, subsidence, Arctic, InSAR, palsa, peatlands

## 1.0 Introduction

Permafrost regions are critical components in the climate system, due to their essential carbon (C) storage service (Harris et al., 2022). The circumpolar permafrost region in particular, stores around  $1300 \pm 200$  Pg of organic C, corresponding to around 50% of the global terrestrial C pool (Hugelius et al., 2020; Köchy et al., 2015). It covers around 21 million km<sup>2</sup> or 22% of the Northern Hemisphere's exposed land surface (Obu, 2021). Northern peatlands themselves store an estimated  $415 \pm 150$  Pg of C in an area covering around 3.7 million km<sup>2</sup> of which around 1.7 million km<sup>2</sup> is permafrost within the circumpolar permafrost region in discontinuous and sporadic permafrost zones (Hugelius et al., 2020). Permafrost in these peatlands raises the surface above the water table forming so-called palsas (pl. palsas) or, in extended form, peat plateaux (Seppälä, 2011). These account for substantial areas of global permafrost, including in northern Fennoscandia (Ballantyne., 2018; Gislén et al., 2017; Tarnocai et al., 2009). In northern Sweden, 137 km<sup>2</sup> of these palsas have been recorded from field reports (Backe, 2014). Climate warming, and the associated alteration in the precipitation regime, is increasingly recognized to be a particular threat to permafrost (Biskaborn et al., 2019), with the subarctic Fennoscandian permafrost region, and the palsas within, particularly vulnerable (Christiansen et al., 2010; Farbroth et al., 2013).

Climatic models project unsuitable conditions for permafrost within the coming century, with the most pessimistic estimates projecting unsuitability even sooner - by 2040 in Fennoscandia (Chadburn et al., 2017; Fewster et al., 2022; Könönen et al., 2022; Stefan et al., 2006). As palsas are often found in the sporadic or discontinuous permafrost zone (Zuidhoff & Kolstrup, 2000), they are particularly sensitive to climate warming and any resultant permafrost thaw and disappearance. Their sensitivity mainly results from the alterations in the thermal insulation effect of peat deposits and snow as the climate changes (Seppälä, 2011; Smith & Riseborough, 1996). Specifically, organic peat has a high thermal conductivity when wet and frozen, but low conductivity when dry and thawed. Snow has a highly insulating effect on ground temperature. Thus, extended periods of air-temperatures below 0°C and thin snow cover in winter are beneficial to maintain or grow the perennial frozen core of palsas and peat plateaux. Low summer precipitation, which reduces the thermal conductivity of peat, also helps to preserve the frozen cores in palsas. In contrast, increased snowfall has been linked to permafrost degradation as it increases winter insulation. Further, high summer precipitation leads to higher thermal conductivity of peat, and combined with warm summer temperatures, can degrade permafrost by increasing permafrost temperatures and subsequent thawing of the frozen peat core of palsas. The strong insulating properties of peat allow the occurrence of permafrost at the southern extent of the northern permafrost region and valley bottoms in areas otherwise too warm for permafrost (Johansson et al., 2013; Seppälä, 2011; Smith & Riseborough, 1996).

Warming of the permafrost in palsas typically leads at the surface, to top-down thaw, (i.e. thickening of the active layer), and eventual subsidence of the surface, as well as lateral thaw, sometimes called abrupt thaw or thermokarst, which occurs at the margin of peat plateaux and palsa edges (Seppälä, 2011; Smith & Riseborough, 1996; Zuidhoff, 2002). This is often associated with water-logged conditions and, as a result, increased methane (CH<sub>4</sub>) emissions (Glagolev et al., 2011; Hugelius et al., 2020; Matthews et al., 1997; Miglovets et al., 2021; Schuur et al., 2009; Turetsky et al., 2020; Varner et al., 2022), which is a central theme for permafrost research (Sjöberg *et al.*, 2020). A subsequent impact of this permafrost degradation is an alteration in vegetation cover, its hydrology, and human use of the landscape (e.g., infrastructure and reindeer husbandry) (Markkula et al., 2019; Ramage et al., 2021). Given the potentially large impacts of permafrost thaw on the global climate, ecosystem function and human activity, quantification and monitoring of the subsidence in peat deposits affected by permafrost thaw and degradation, as well as an understanding of their sensitivity to changing climatic parameters, is urgently required (IPCC, 2021).

The degradation of the permafrost of palsas has been observed right across the circumpolar permafrost region in a number of studies, including in northern Scandinavia (Åkerman & Johansson, 2008; de la Barreda-Bautista et al., 2022; Luoto & Seppälä, 2003; Olvmo et al., 2020; Sannel et al., 2016; Varner et al., 2022); Russia (Glagolev et al., 2011; Miglovets et al., 2021; van Huissteden et al., 2021); the USA (Douglas et al., 2021; Douglas et al., 2015; Sannel, 2020) and Canada (Mamet et al., 2017; Sannel & Kuhry, 2011; Short et al., 2014; Vallée &

Payette, 2007). Although rapid degradation in response to short term climatic events has been observed, typically permafrost degradation has been investigated via long-term monitoring at decadal timescales in response to changes in temperature and precipitation conditions (Åkerman & Johansson, 2008; de la Barreda-Bautista et al., 2022; Olvmo et al., 2020; Sannel et al., 2016). These longer-term studies have shown strong relationships between permafrost degradation and summer temperatures, length of the thaw period, winter precipitation and snow depth (Smith et al., 2022). These types of analyses are very useful for quantifying how much of the landscape has already transitioned and understanding the climate change drivers behind these changes, but they do not capture the initial stages of permafrost degradation in palsas and the lower rates of subsidence that have yet to result in observable changes in the vegetation or thermokarst formation. The latter is crucial to understand the ongoing response of palsas to climate warming and to predict when pulses of greenhouse gases to the atmosphere and other impacts (e.g., on infrastructure) are likely to occur. Thus, we need approaches that detect early signs of degradation at landscape scales, with repeated observations.

Due to the vast extent and remoteness of permafrost areas there is no current complete annual degradation rate measurements. So, we looked to satellite remote sensing to underpin the measurement and monitoring assessment of permafrost peatlands, their degradation and resultant climate impacts (Hugelius et al., 2020; Swingedouw et al., 2020). Optical remote sensing approaches can be augmented with RaDAR remote sensing methods, including InSAR, to capture the early response of permafrost to warming. These methods can detect vertical land surface motion at millimetre precision across a range of natural landscapes, with greater confidence in the direction of surface motion than the absolute magnitude (Alshammari et al., 2020; Alshammari et al., 2018; Bartsch *et al.*, 2016; de la Barreda-Bautista et al., 2022; Short et al., 2014; van Huissteden et al., 2021). The regular sampling frequency, insensitivity to cloud and, in the case of Sentinel-1, low cost, means InSAR from Sentinel-1 should be well suited to measure and monitor ongoing changes in permafrost affected by climate change. Further, Sentinel-1 for InSAR is effective at both local and regional scales - the 20m × 20m spatial resolution enables measurement of surface motion within local sites (de la Barreda-Bautista et al., 2022), and can do so over entire and complex landscapes, such as the circumpolar permafrost region (Reinosch et al., 2020).

The overall aim of this study was to carry out a regional-scale analysis of permafrost degradation across the palsas of northern Sweden, principally using Sentinel-1 InSAR-derived subsidence as an indication of degradation. Pertinent to this is that any InSAR-detected changes can be associated with known and delineated targets in the wider landscape. Furthermore, it is also important to understand any within-site dynamics of permafrost degradation. This paper therefore has specific objectives to: (i) measure the subsidence rate between 2017-2021 of all major palsa complexes in the northern Sweden region; (ii) determine in which palsa complexes subsidence is greatest, and (iii) assess if the spatial patterns of degradation can be linked to climatic variables and properties of the different sites across the region. To achieve these objectives, we combined large-scale regional analysis with higher resolution site-specific analysis of patterns in subsidence, using a combination of datasets - satellite (Sentinel-1) InSAR; occupied airborne optical and LiDAR data; and snow depth, precipitation, and temperature time-series from meteorological stations across the region.

## 2.0 Methodology

### 2.1 Study area

This study focused on the northern part of Sweden; a region containing palsa, located between 68.84-67.64° N and 18.71-21.19° E. The palsas of the region are confined predominantly to valley bottoms in an elevation range between ca. 350 and 590m asl (Fig. 1). The rest of the study area region is comprised of forests and/or mountain land covers (Siewert, 2018; Åkerman & Johansson, 2008). Of all the palsas in the region, the eight largest complexes of concentrated palsa range between 50 and 273ha in area (Table 1). These were located across the region, which covers a ca. 20,000km<sup>2</sup> area, with the largest palsa sites located north-west. Smaller palsas occur scattered in distribution right across the region. The climate varies from north to south ([www.smhi.se](http://www.smhi.se)). The mean January and July temperatures in Karesuando in the northern part is -16 and 12.8°C, respectively, while in Kiruna, slightly further south, the mean January, and July temperatures is -11.6 and 13.4°C (1991-2020 average). Mean annual precipitation is 443 and 560mm in Karesuando and Kiruna, respectively.

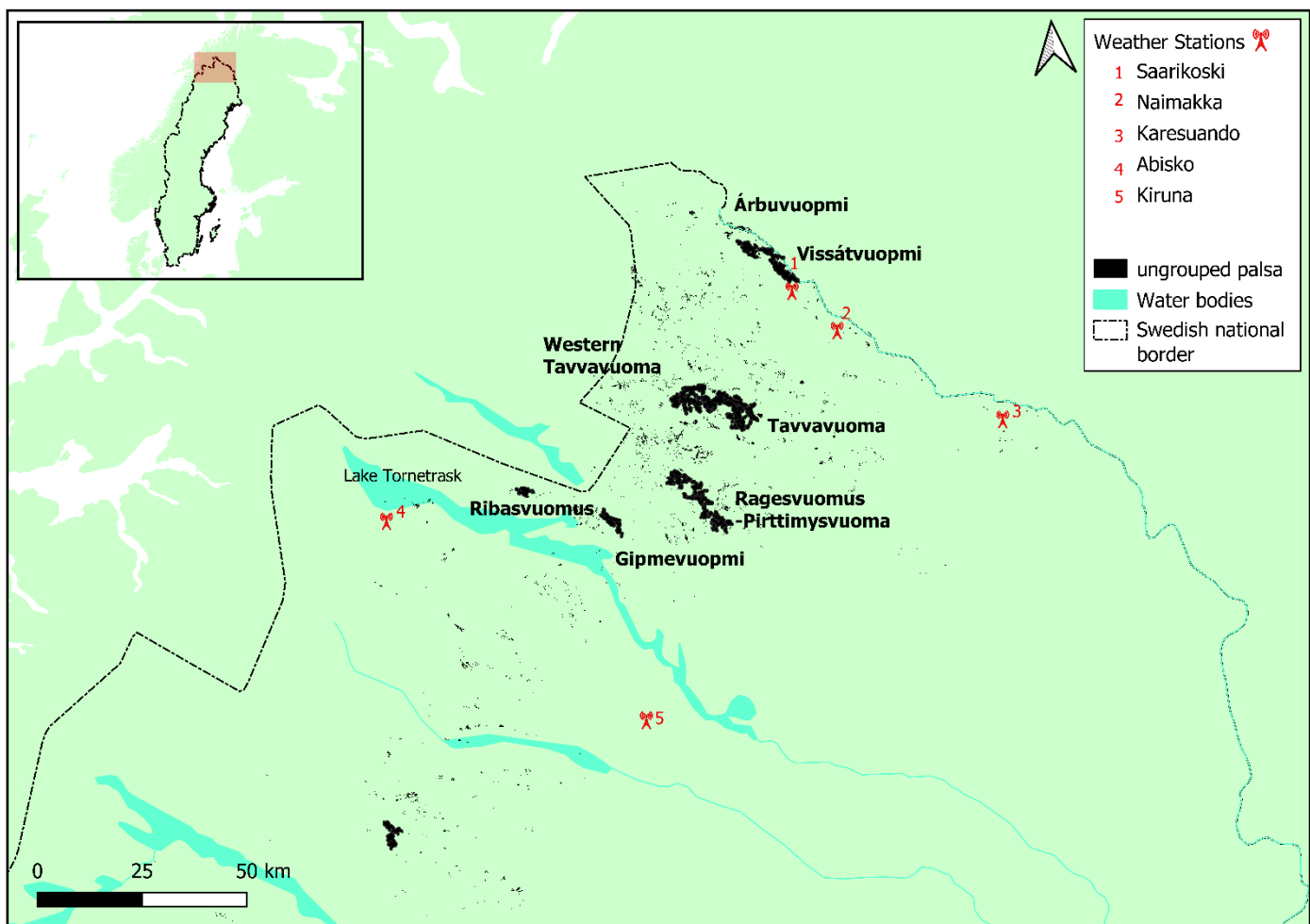


*Figure. 1: Map of the palsa in Sweden which were investigated in the study focusing on the eight named palsa complexes. The black regions show all the palsa which has been reported to exist (Backe, 2014,) with the larger named areas displaying the 250m buffers around the palsa areas which have created continuous expanses. Meteorological station positions used in the study are also indicated.*

A previous national palsa mapping dataset provided raster cells at a spatial resolution of 100m, with the % palsa cover computed and a 250m buffered output to provide continuous palsa area outputs (Backe, 2014). This afforded analyses at a spatial resolution suitable for analysis with Sentinel-1 yet provide practical representation of the condition of the palsa in this region. All these data were analysed in this study, but the eight largest

continuous areas of these palsa (Backe, 2014) were focused on, hereon in referred to as palsa complexes, a term reflecting their mosaic nature of raised palsa and/or peatland plateaux, interspersed with lower lying fen or thermokarst areas. These eight sites account for the majority of the palsa areas in Sweden, the sites are listed in Table 1 along with some associated information on their status and total and raised palsa plateaux areas.

*Table 1: Information on the major palsa complexes analysed in this paper (Backe, 2014). The protection status means no or limited direct anthropogenic activities that may influence palsa degradation. Total site area is calculated from the total number of 100m × 100m palsa pixels at each site - these pixels have associated percentages for how much of the 100m x 100m area is palsa. The average of these percentages for each site displays the palsa density at each site. These percentages are then used to calculate the “total palsa area” for each site based on the original report estimates.*

Site Name	Protection Classification	Total site area (ha)	Average extent palsa in these areas (%)	Total palsa area (ha)	LiDAR Collection year	Central location (Latitude, Longitude)
Árbuvuopmi	Not protected	327	26.3	86.06	2018, 2016	21.03464, 68.83842
Vissátvuopmi	Not protected	867	31.6	273.75	2015, 2018	21.19497, 68.79412
Tavvavuoma	EU Natura 2000 SPA, SAC. Site of National Importance for Nature conservation	1719	15.8	271.25	2018	20.85043, 68.51132
Western Tavvavuoma	EU Natura 2000 SPA, SAC. Site of National Importance for Nature conservation	813	13.0	105.74	2018	20.57727, 68.53953
Gipmevuopmi	Pristine mountain forest, Nature reserve, EU Natura 2000 SCI	303	23.0	69.62	2013	20.09767, 68.28377
Ragesvuomus-Pirttimysvuoma	Pristine mountain forest, Nature reserve, EU Natura 2000 SCI	881	6.55	57.74	2013	20.48660, 68.3741
Sirccam	EU Natura 2000 SCI	397	12.8	50.70	2015	18.71528, 67.64537
Ribasvuomus	Pristine mountain forest, Nature reserve, EU Natura 2000 SCI	216	23.2	50.13	2014	19.60100, 68.36116

## 2.2 Datasets

The InSAR-derived dataset of surface motion over this northern Sweden region of study was calculated for the period between 2017 to 2021, from single look complex (SLC) C-band SAR data, captured in Interferometric Wide (IW) Swath mode by the Sentinel-1 constellation (European Union’s Copernicus Programme; Torres et al., 2012). SAR data input were from the thaw season when there was minimal coverage of snow and ice (i.e., between April and October in each year). Data from descending tracks 168 and 66 were used to cover the target area. Four stacks were processed independently with one from track 168 and three from track 66, which was split into a northern, middle, and southern subsets. The APSIS (formerly ISBAS) method (Sowter et al., 2013; Sowter et al., 2016) was used to characterize surface motion which relaxes the need for consistent phase stability and therefore enables near-complete spatial and temporal coverage over vegetated surfaces (Alshammari et al., 2020; Alshammari et al., 2018; Bradley et al., 2022; Cigna & Sowter, 2017; Gee et al., 2017; Sowter et al., 2016), including those found across snow-free permafrost regions.

InSAR processing of Sentinel-1 IW SLC imagery involves a series of steps summarised in Figure 2. Firstly, deburst and merging involved combining individual sub-swaths into a single wide-area SLC product. Secondly, the process of deramping produced a product where the problem of an ambiguous and rapidly changing phase with azimuth was solved for; a specific deramping function is available for Sentinel-1 data (ESA, 2015). Next step involved the co-registration of each Sentinel-1 image to a common slant range coordinate system and multi-

looking of data by factors of 5 m in range and 20 m by azimuth. This produced a dataset with an approximate spatial resolution of  $20\text{m} \times 20\text{m}$ . Using a perpendicular baseline of 250m and maximum temporal baseline of 183 days  $\sim$  2100 interferograms were generated per stack. The temporal baseline was chosen to balance the need to reduce the baseline to minimise phase ambiguities and best maintain coherence across the region, whilst also using a baseline long enough to generate season-to-season pairs over consecutive years. This is required over permafrost regions to capture more subtle trends of surface motion during the thaw period (de la Barreda-Bautista et al., 2022; Liu et al., 2010). The interferograms were unwrapped using a modified version of the SNAPHU algorithm (Shen et al., 2002), which converts circular phase data into a linear measure of deformation. The algorithm was modified in order to allow the ability to parallelise and to spread the calculation across multiple cores (Chen and Zebker, 2002). The multi-annual average velocity was calculated for pixels which maintained a coherence greater than 0.45 in a minimum of  $\sim$  650 interferograms, with respect to stable reference points located in the town Kautekenio ( $N^{\circ}69.00$ ,  $E^{\circ}23.04$ ) for track 168 and Narvik ( $N^{\circ}68.44$ ,  $E^{\circ}17.42$ ), Kvikkjokk ( $N^{\circ}66.95$ ,  $E^{\circ}17.72$ ), and Rognan ( $N^{\circ}67.09$ ) for the subsets of track 66. The line-of-sight measurements were converted to vertical surface displacement using a cosine correction and finally mosaicked into a single deformation product. Localised UAV studies at sites in Sweden have verified the ability to use InSAR as a tool to monitor permafrost degradation (de la Barreda-Bautista et al., 2022).

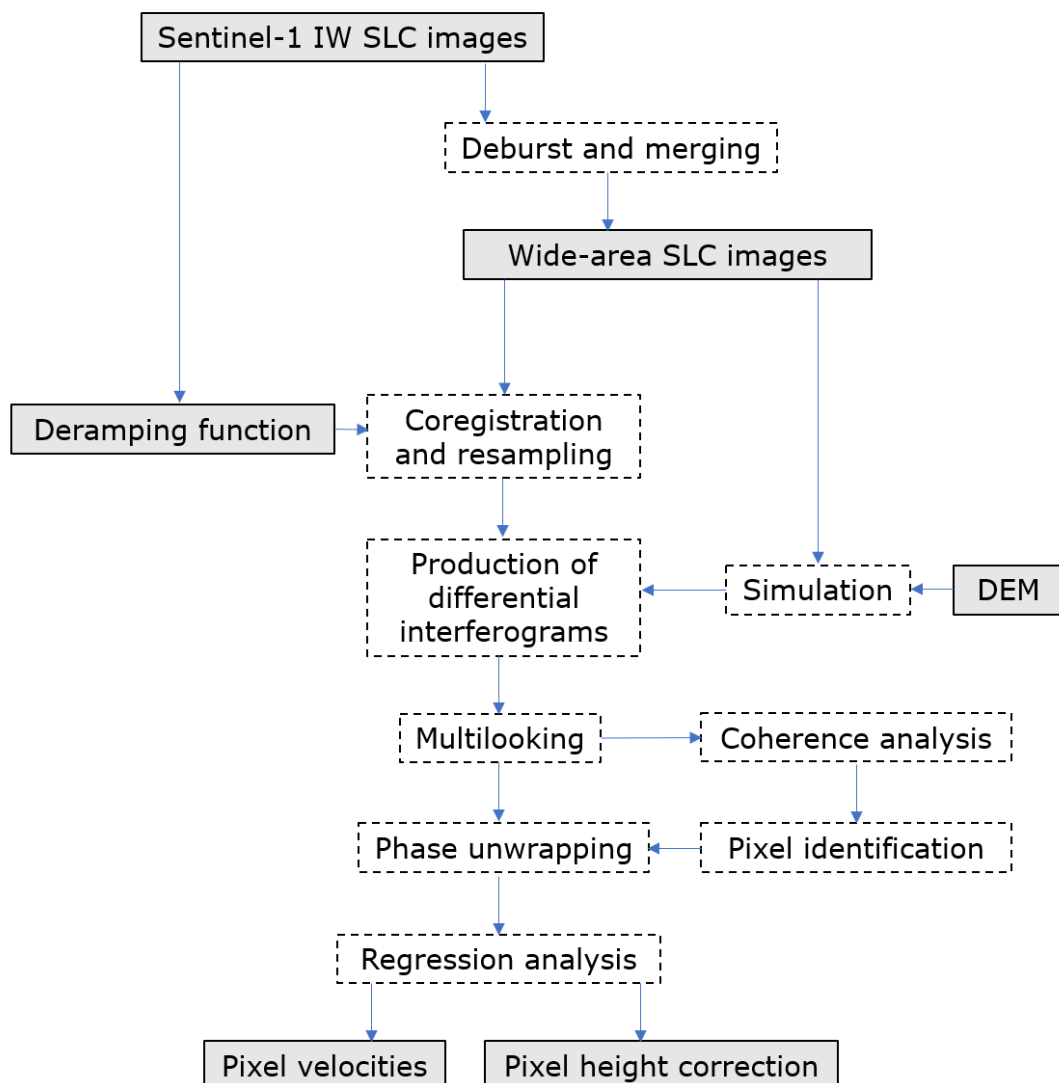


Figure 2: A flowchart summarising the steps undertaken for InSAR processing using the APSIS method to create a surface motion product from Sentinel-1 IW SLC imagery. Boxes shaded grey represent data sets, boxes with dotted borders represent processing steps. Modified from Sowter et al. (2016).

In order to interpret the resultant surface motion dataset produced by the ASPIS InSAR method, two sets of additional data were sourced: (i) higher resolution remote sensing data and (ii) meteorological data. The former included orthophotos captured of the eight target areas by occupied airborne surveys commissioned by the Swedish Mapping, Cadastral and Land Registration Authority ([www.lantmateriet.se](http://www.lantmateriet.se); © Lantmateriet). The orthophotos (Lantmateriet, 2021) have scenes covering a 5km × 5km area, at a 0.5m spatial resolution, the majority were captured in 2021, although gaps were filled with imagery from 2018 for two sites. The Swedish National Digital Elevation Model (DEM), was also used in this study. The DEM was derived via occupied airborne LiDAR data capture between 2013 and 2018 (Table 1) processed to compute elevation at 2m spatial resolution across Sweden ([www.lantmateriet.se](http://www.lantmateriet.se); © Lantmateriet). The orthophotos and DEM provided elevation and landscape characteristics (geomorphic features) for use in this study. The meteorological data was captured by the Swedish Meteorological and Hydrological Institute ([www.smhi.se](http://www.smhi.se)) at meteorological stations across the region. Specifically, the air temperature, precipitation, and snow depth data, were sourced and used from specific stations, i.e., those located closest to the palsa complexes under investigation namely at Abisko, Kiruna, Karesuando, Saarikoski, and Naimakka (Fig. 1).

## 2.3 Data analyses

### 2.3.1 Surface motion statistics

The ASPIS InSAR surface motion dataset was clipped to the 100m x 100m spatial resolution of the whole palsa dataset and separately to the eight palsa complexes (Backe, 2014). From this the frequency distributions of ASPIS InSAR surface motion at these eight palsa complexes, and over all individual palsa peatland raster cells in the region, were produced. Using these data, the maximum and minimum rates of surface motion at each site was determined, as well as the sum of the pixels with palsas that showed subsidence. These derived data relating to surface motion were further interpreted using the orthophotos and DEMs, supported by the meteorological data.

### 2.3.2 Roughness thresholds

The DEM tiles were joined together and clipped to the eight palsa complexes. Following this, the degree of elevation roughness was calculated, via the native topographic roughness index function (Riley, DeGloria, & Elliot, 1999). This roughness index was thresholded at > 0.5 to provide a visual depiction of palsa landform edges in the otherwise typically even terrain of the valley bottoms where the palsas occur. The roughness data was visually compared to the orthophotos from a subset of areas to assess its potential for delineating palsas and this allowed us to determine a threshold value that connected these continuous terrain variables to the specific features of the palsa complexes, such as the raised mound structure of the palsa – so-called palsa mounds (Franklin, 2020). Hillshade was also calculated via the native QGIS function using the default formula, which uses a lighting effect to visualise the roughness of the terrain from differences in local elevation (QGIS, 2022). The roughness, hillshade, and elevation outputs were overlaid on the mapped palsa tiles to provide higher resolution visual interpretation.

### 2.3.3. Causes of surface motion

To test for the causes of surface motion palsa ASPIS InSAR surface motion was compared against roughness, elevation and palsa percentage provided with the palsa raster cells (Backe, 2014). The roughness, elevation and InSAR outputs were resampled to the resolution of the mapped palsa tiles (100m x 100m) to enable statistical comparison. The zonal statistics tool was used to extract mean average values from the resulting roughness and elevation outputs for the 100m spatial resolution mapped palsa tiles.

To analyse the relationships between surface motion, roughness and percent palsa in each 100m by 100m pixel stratified by palsa complex, SciPy statistics (Virtanen et al., 2020) was used to obtain Pearson's correlation statistics with an alpha value of 0.05 used to test for significance. Pandas (McKinney, 2011) and NumPy (Harris et al., 2020) were used for data management. All scripts are available on the project GitHub ([https://github.com/SamValman/Permafrost\\_Sweden](https://github.com/SamValman/Permafrost_Sweden)).

#### 2.3.4 Climatic factors

Mean annual, maximum, and minimum daily air temperature, precipitation, and depth of ground snow for the period 2000 to 2022 from the meteorological station nearest to a correspondent palsa complex were extracted and analysed. The Naimakka station did not record snow depth and the Saarikoski station did not record air temperature, however, it was deemed that at the regional scale of this study these sites were sufficiently close together (18km) to be interchangeable. Subsequently, data was averaged to provide an annual measurement of each meteorological variable for each station/palsa complex. Due to incomplete meteorological datasets, a longer-term record of the meteorological variables was not possible for all sites. However, long-term climate data (>100years) was available from three meteorological stations in the region: namely, Karesuando, Kiruna, and Abisko. This data was used to assess temporal variability in annual, winter (December, January, and February (DJF)) and summer (June, July, and August (JJA)) temperature, precipitation and snowfall since the start of records across the region. Descriptive statistics (mean, minimum, maximum and inter-quartile range) were produced to express the regional differences between these sites. Lastly, to complement the point based meteorological (both weather and climate) data, we used modelled permafrost probabilities based on climatic conditions to explore relationships between climatic conditions (Obu et al., 2018) and subsidence rates. In this context, it is worth noting that there may be a mismatch between the modelled permafrost distribution and permafrost in palsa areas as this can, in some areas, be a relic of cooler climatic conditions. We used the mean values from the roughness and InSAR data to resample to 100m spatial resolution in line with the permafrost raster cells and spatially joined the permafrost probability layer, taking the mean value where the 100m cell straddled multiple permafrost probability cells.

The relationship between the meteorological variables both over the last two decades at the weather stations closest to the palsa complexes and duration of the climate record at the three weather stations with the longest data series were assessed using linear regression analysis in Genstat (VNS Ltd). Assumptions of normality and homogeneity of variance of the residuals were assessed using residual plots in Genstat. Some of time series were incomplete, in these instances the analysis was conducted using the slightly shorter time series (see fig. 8).

### 3.0 Results

#### 3.1 Surface motion

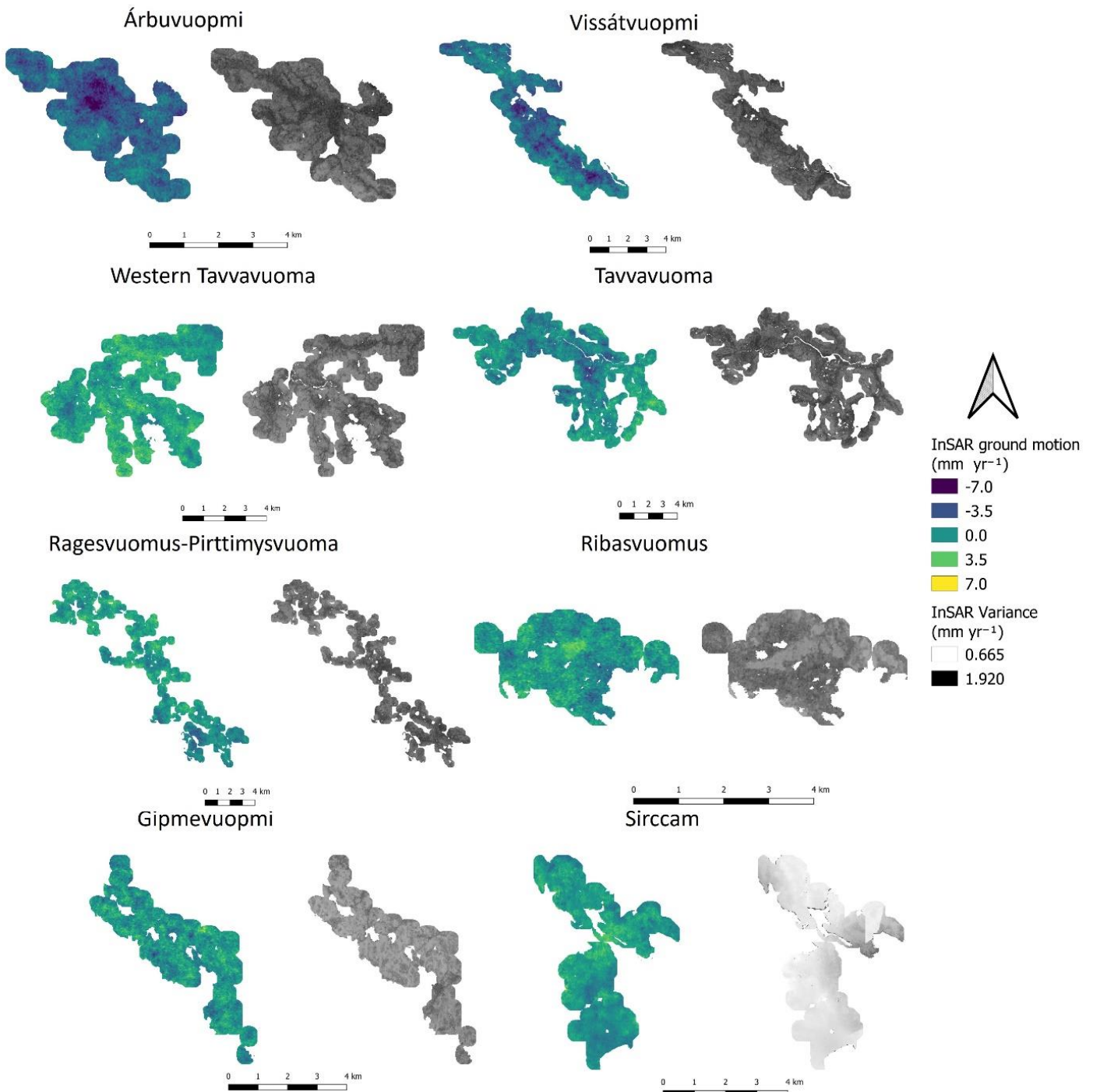
The ASPIS InSAR-derived surface motion outputs for the time-period of interest (2017-2021), ranged between -9.9 and 7.7mm yr<sup>-1</sup> across all of the palsa raster cells measured in northern Sweden, with a mean of 0.05, median of 0.2 and range of 17.7mm yr<sup>-1</sup>. Focusing solely on the eight palsa complexes provided greater insight and excluded the most extreme uplift values from scattered individual palsas (Table 2). 69% of results were within MSE of changing ground motion direction.

*Table 2: InSAR subsidence and uplift measurements of the palsa complexes defined in Figure 1 and Table 1. The total palsa area were used to isolate and extract ASPIS InSAR measurements of surface motion at each of the eight sites.*

Site	Max subsidence (mm yr <sup>-1</sup> )	Max uplift (mm yr <sup>-1</sup> )	Subsiding area (ha)	Area subsiding >3.5 mm yr <sup>-1</sup> (ha)	Mean standard error (mm yr <sup>-1</sup> )
Árbuvuopmi	-9.9	1.7	321.3	138.4	1.5
Vissátvuopmi	-8.9	3.5	796.2	204.8	1.5
Tavvavuoma	-6.4	6.6	1009.4	50.9	1.4
Western Tavvavuoma	-5.1	6.3	215.0	1.0	1.4
Gipmevuopmi	-6.9	6.3	117.2	1.8	1.2
Ragesvuomus-Pirttimysvuoma	-5.9	5.7	358.6	7.4	1.4
Sirccam	-3.1	5.4	135.3	0.0	0.9
Ribasvuomus	-6.5	5.5	93.6	0.7	1.3



275 The spatial plots of surface motion for each palsa complex displayed in Figure 3, illustrates patterns of surface  
 276 motion (both subsidence and uplift and associated variance) across this northern Sweden region. This is evident  
 277 both within the palsa complexes and between the complexes.



278 *Figure. 3: Palsa ground motion measured using Satellite InSAR from 2017 to 2021, showing differing levels of*  
 279 *degradation across the eight study sites. Sites are ordered by their latitudinal position. Negative values*  
 280 *correspond to subsidence. Note that in order to plot continuous areas the scenes shown are the palsa area plus*  
 281 *a 250m buffer around each 100m × 100m raster cell that cover a minimum of 1% palsa (Backe 2014). This*  
 282 *means that areas of non-palsa peatland and some areas with mineral soil are included in the figure. ASPIS*  
 283 *InSAR variance were less than 1.5mm yr<sup>-1</sup> in over 90% of pixels.*

284

Across the target sites 3046.6ha (Table 2) out of the total site area of 5523ha (Table 1) were subsiding, which equates to ca 55% of the total palsa complexes' area. Out of the subsiding parts of the palsa complexes, 405ha were subsiding at rates  $>3.5\text{mm yr}^{-1}$  at near gaussian distribution. However, it is evident from the frequency distribution plots, that it is in the palsa complexes in the far north of the region that subsidence dominated the surface motion measured (Table 2, Fig. 4). At Vissátvuopmi and Árbuvuopmi 98 and 92% of the palsa complexes were subsiding with maximum subsidence rates of  $-9.9$  and  $-8.9\text{mm yr}^{-1}$ , respectively. The measured area affected by high subsidence rates of between ( $>3.5\text{mm yr}^{-1}$ ) were 204.8ha and 138.4ha at Vissátvuopmi and Árbuvuopmi, respectively. This means that ca. 30% of the total combined area of these two sites (1194ha) is in the highest range of subsidence. The high degree of palsa subsidence at Vissátvuopmi and Árbuvuopmi was confirmed by field observations at these sites (Sofie Sjogersten, pers. Obs.): Both sites showed signs of active lateral erosions, large scale subsidence and thermokarst formation. The more southerly sites also show subsidence, although ground motion rates were much more stable, with the  $-1$  and  $1\text{mm yr}^{-1}$  range being most common (Fig. 4). Areas further to the south and west showed signs of uplift, particularly the western parts of Tavvavuoma and Ribasvuomus with maximum rates of uplift of  $6.3\text{mm}$  across some smaller parts of these sites. However, all sites have some degree of subsidence, albeit at a lower rate compared to the heavily subsiding northern sites.

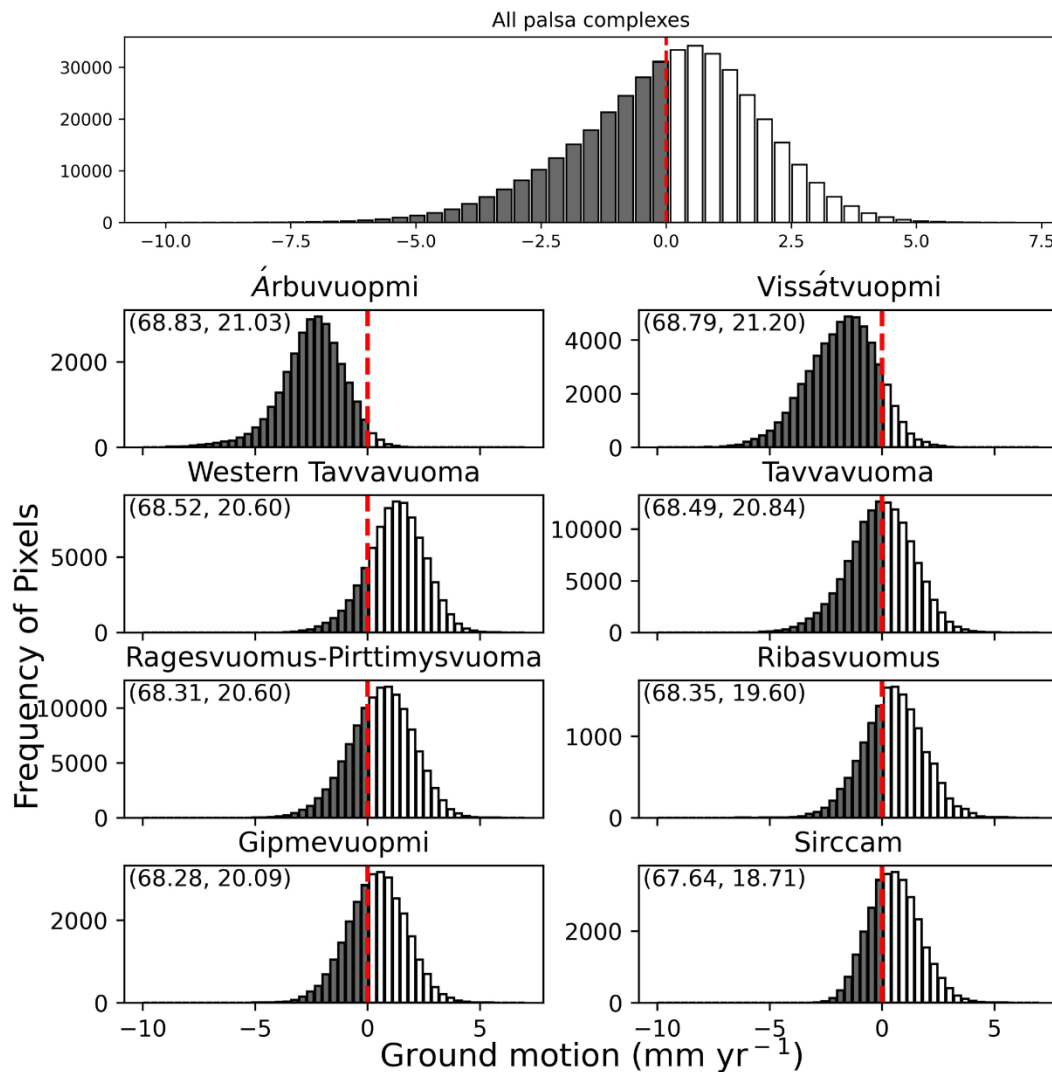


Figure 4: Distribution of 20m x 20m ASPIS InSAR pixels within each of the palsa complexes in this study and the overall trend of the dataset according to the distribution of pixel moving in a particular direction and a given rate. Shaded areas with negative values correspond to subsidence. The dashed central lines indicate pixels in stable areas with no motion. Central point latitude and longitude is provided for each site in brackets for each site.

### 3.2 Topographic drivers and indicators

Calculating the roughness index from the DEMs at each palsa complex enabled differentiation of palsa from surrounding lower lying and flat fen areas. Representative example complexes are shown in Figures 5 and 6 - Vissátvuopmi and Western Tadvavuoma. Overall, the palsa complexes to the north (e.g., Fig. 5b, c) display a more pronounced topography across the focus areas than the more south-westerly ones (e.g., Fig. 6b, c). There was clear correspondence between density of palsa and subsidence, i.e., areas with more palsa showed more subsidence (Fig. 5a, d). Furthermore, the palsa complexes showed greater elevation variation compared to surrounding fen areas and were more densely clustered to the north than in the more south westerly sites. These features spatially coincided with higher subsidence. Substantial within site variability in subsidence was evident, where the pixels with the highest subsidence rates being clustered together and following landscapes features, e.g., palsa plateau edges. It was evident that many separate palsa complexes in an area resulted in a high degree of elevation change, causing a high roughness index. In turn, areas with high roughness have the greatest subsidence (Fig. 5,6). Visual comparison between orthophotos and roughness showed that areas of high roughness corresponded well with areas of severe permafrost degradation (as indicated by lateral erosion and thermokarst formation).

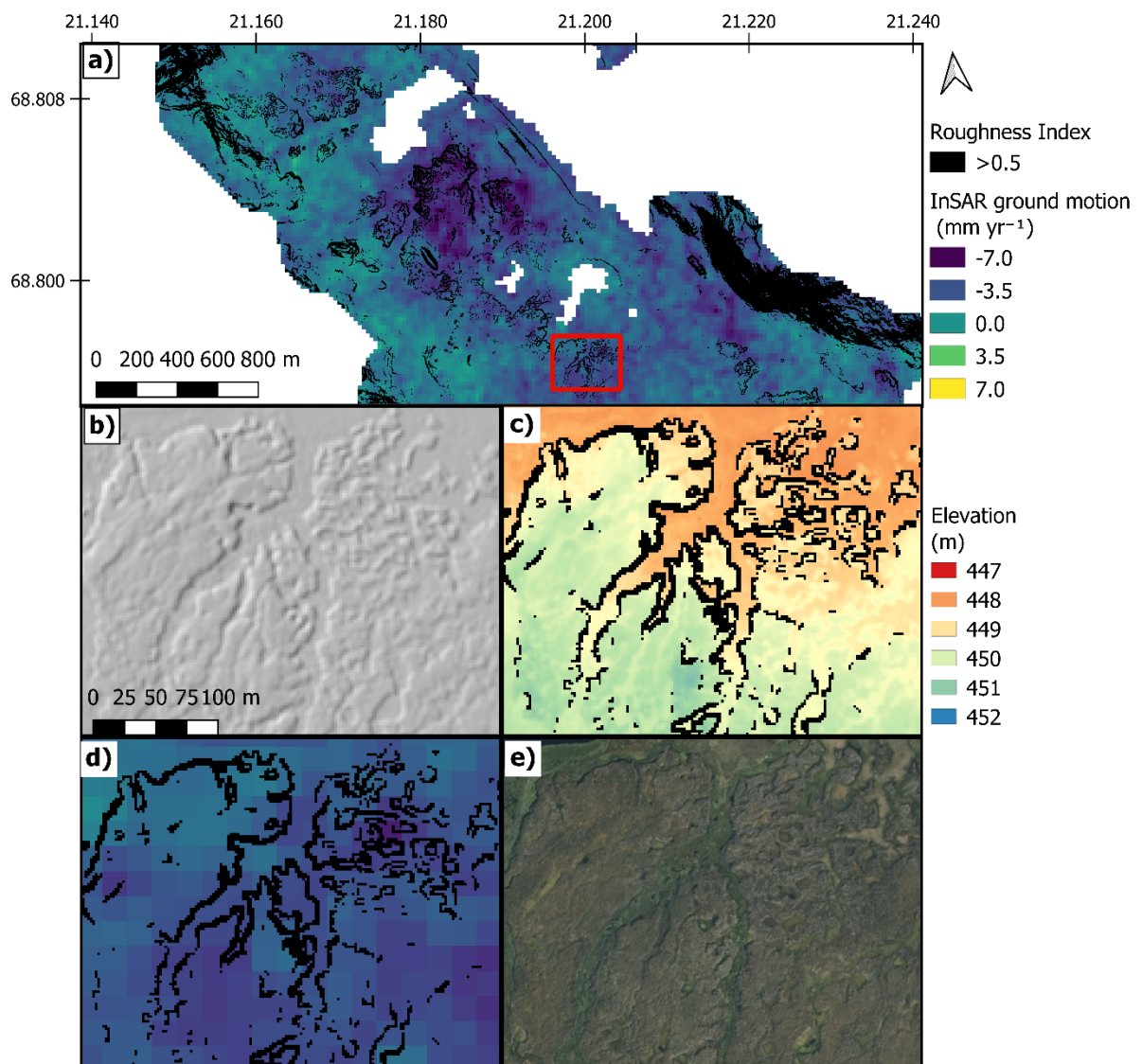


Figure 5: Visual analysis of Vissátvuopmi one of the sites where the most subsidence was found to be occurring. Evaluation of correspondence of hillshade DEM (b), DEM (c) and a close look at InSAR subsidence (d) with palsa complexes suggested by roughness overlays and aerial imagery (e). The positioning of b,c, and d within the larger site (a) show bands of subsidence proximal to roughness patches suggesting palsa.

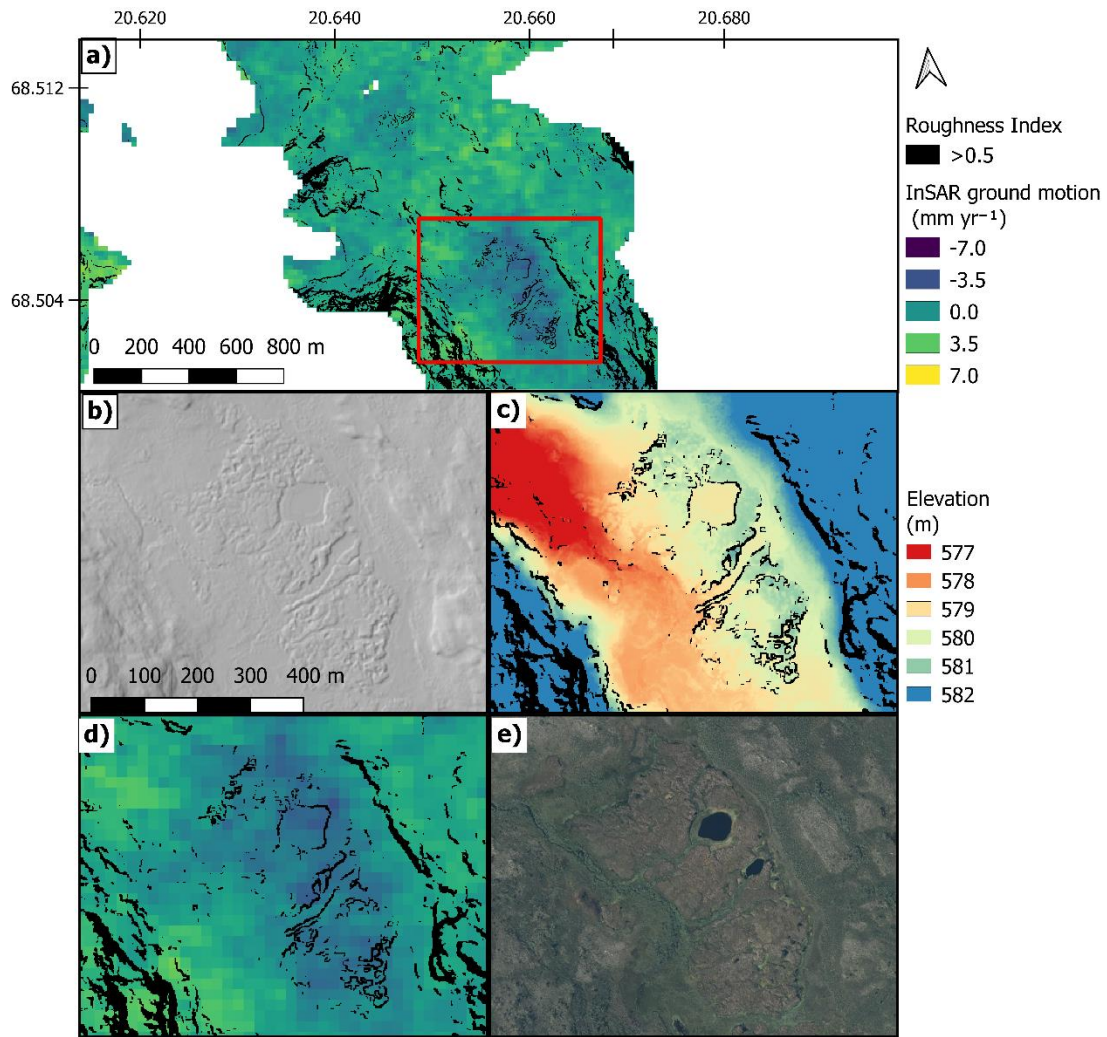


Figure 6: Visual analysis of Tavvavuoma which was found to have much lower levels of subsidence in comparison to more northern sites. Evaluation of correspondence of hillshade DEM (b), DEM (c) and InSAR subsidence (d) with Palsa complexes suggested by roughness overlays and aerial imagery (e). The positioning of b, c, and d within the larger site (a) show many less “bands” (linear arrangements of palsa across the image) of subsidence and potential palsa than Figure 4.

Regression analysis showed a relationship between roughness and subsidence as sites with greater subsidence were also found to have greater roughness (Fig. 7a). Higher percentage palsa in a location was linearly related to subsidence with the greatest subsidence found in areas with the highest percentage palsa cover (Fig. 7b). It was also clear that the modelled permafrost probability did not correspond to the percentage of palsa, i.e. pixels with 100% palsa are in some instances predicted to have no permafrost (Fig. 7b).



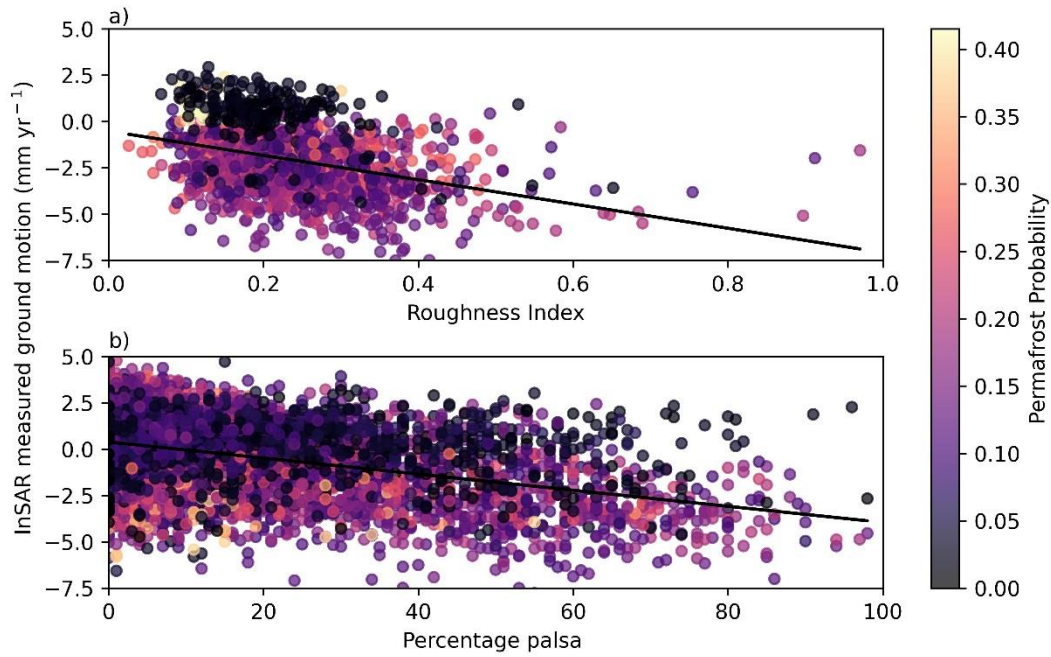


Figure 7: Relationship between a) the roughness index;  $p < 0.001$ ,  $R^2 = 0.35$  and b) percentage palsa in a pixel;  $p < 0.001$ ,  $R^2 = 0.41$  and subsidence. The colours indicated for each data point are the analysed probability (on a scale from 0 to 1) that an area would include permafrost, (Obu et al., 2018). Note that there is less data for the analysis of roughness as the roughness was characterized only for the eight study sites and not all palsa raster cells from (Backe, 2014). Roughness values from valley sides (which at time were included in the buffer areas) are not used in the figure.

### 3.4 Meteorological trends

The analysis of the meteorological data showed variability in both weather and climate across the study region in part reflecting the patterns in the subsidence data. The warmest minimum and maximum temperatures, -29.2 and 32.8°C respectively, were recorded for the palsa complexes north of Lake Tornetrask, i.e. Gipmevuomi and Ribasvuomus (Abisko weather station) (Fig. 1). The temperature in the area of Árbuvuopmi, Vissátvuopmi, and Tavvavuoma palsa complexes (Saarikoski/Naimakka and Karesuando weather stations) ranged between -39.4 and 30.5°C (Table 3, Fig. 8a). The sites had comparable annual snow depth with a mean of 20-30cm (Table 3, Fig. 8b).

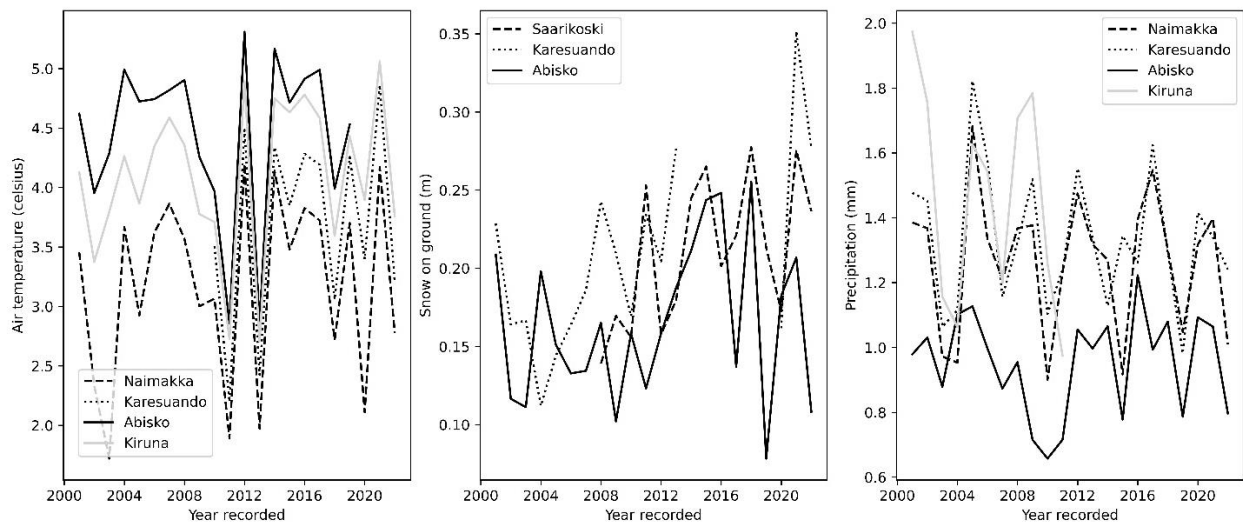


Figure 8: Mean annual a) daily maximum temperature, b) snow depth on the ground, and c) daily precipitation at the meteorological stations in the study region (SMHI 2022).

Table 3: Temperature and snowfall descriptive statistics. The snow depth data are estimated from days with snow on the ground. Mean annual temperature and precipitation are averaged from 2000 to 2021. Maximum, minimum and the inter-quartile range are of daily maximum temperature and daily precipitation since 2000 are also shown. Some weather stations lack certain years but were considered to have adequate coverage for this task while two sites did not have sufficient data collection during the time period to be reliable and were shaded out.

Weather Station	Temperature (°C)				Snow depth (m)			Precipitation (mm)		
	Mean annual	Max daily	Min daily	IQR daily	Mean annual	Max daily	IQR daily	Mean annual	Max daily	IQR daily
Naimakka	-1.40	29.5	-38.2	15.7				456	50.8	1.0
Saarikoski					76.9	0.85	0.43	422	43.6	0.9
Karesuando	-0.70	30.5	-39.4	16.9	75.1	1.00	0.40	490	53.2	1.1
Abisko	0.53	32.8	-29.2	13.5	60.0	1.27	0.42	348	61.9	0.6
Kiruna	0.06	30.3	-30.6	15.6	5.3	1.13	0.45	545	53.1	0.9

There was no detectable difference in climatic trends among the meteorological weather stations since 2001 for any of these sites ( $p > 0.05$ ). In contrast, the longer-term climate records show a strong increase in winter precipitation over the last 140 years at Karesuando, the northern most weather station of the three with long term records available ( $F_{1,136}=122.33$ ,  $p < 0.001$ ;  $\sigma^2=47.0$  %; Fig. 9a). This long-term trend was also evident, albeit less strong, in Kiruna ( $F_{1,110}=28.17$ ,  $p < 0.001$ ;  $\sigma^2=19.7$  %; Fig. 9b). In Abisko, the pattern of increasing in winter (DJF) precipitation was less clear ( $F_{1,108}=8.29$ ,  $p < 0.01$ ;  $\sigma^2=6.3$  %; Fig. 9c). Mean annual Snow depth, temperature, and summer precipitation (JJA) did not show clear temporal trends (See supplementary materials).

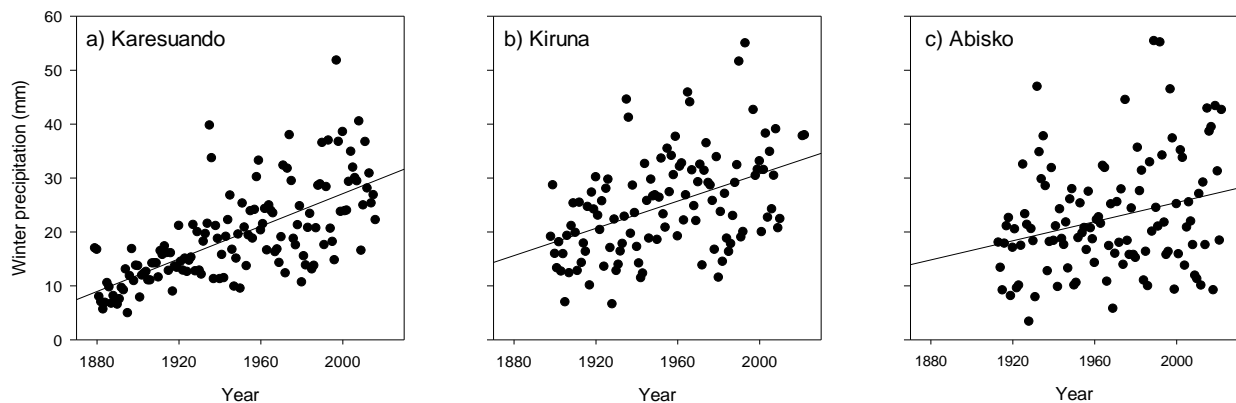


Figure 9. Mean winter (DJF) precipitation over time at a) Karesuando, b) Kiruna, and c) Abisko, significant trendlines are shown.

#### 4. Discussion

By way of satellite ASPIS InSAR-derived surface motion and associated spatial and statistical analyses, we have demonstrated on-going subsidence in the palsas of northern Sweden driven by a warming climate. Based on the compelling agreement of subsidence with palsa landforms and their roughness, we interpret this as permafrost degradation, i.e., thaw of the permafrost core within palsas and disintegration of these landforms. This is in line with a wide range of literature (see introduction) and concurs with the local-scale studies in the area undertaken using both satellite- and field-based methods (de la Barrera-Bautista et al., 2022; Olvmo et al., 2020; Sannel, 2020; Sannel et al., 2016; Sannel & Kuhry, 2011). The findings also agree with what is expected from the severe climate warming impacts on temperatures and precipitation noted in the region (Hänsel, 2020;

Irannezhad et al., 2017; Vikhamar-Schuler et al., 2016) and the modelled predictions of total loss of permafrost across the region within decades (Fewster et al., 2022). We suggest that the surface subsidence of the sample palsa complexes measured in this study, together with complementary work in Norway (Borge et al., 2017), can be taken as evidence of substantial permafrost degradation in many palsa areas across northern Sweden and therefore, likely to be also occurring across northern Fennoscandia

The processes driving the degradation of the permafrost, as measured by the ASPIS InSAR-derived subsidence data, are complex. Although permafrost degradation was observed in all the palsa complexes, rates varied both within and among palsa complexes (Table 2, Fig. 3 and 4). Overall, the InSAR subsidence data demonstrates a south to north gradient in increasing degradation. This indicates that local factors, such as local climate warming responses or permafrost temperature, determine the sensitivity of particular areas and that regional climatic gradients play a role in the long-term trajectory of these ecosystems (Johansson et al., 2011; Olvmo et al., 2020). In particular, winter precipitation is generally considered a strong predictor of permafrost degradation due to the highly insulating properties of snow, preventing heat dissipation during winter (Olvmo et al., 2020; Seppälä, 2011). This points to increased winter precipitation in the part of the northern most part of study areas as a driver of the higher subsidence rates at the northern most palsa complexes (Table 2 and Fig. 8a). Interestingly, climate data from the last two decades did not reveal strong differences in climatic conditions over the area. This suggests that long-term trends combined with a buffered system reaction to change are driving regional patterns in permafrost degradation.

It could also be the case that the observed north to south gradient of subsidence rates reflect different phases of progression in an ongoing trend of permafrost degradation across the study region of northern Sweden. It is plausible that the degradation process has progressed further at the more southern sites, reflecting higher permafrost temperatures, and that as a result, subsidence rates have now slowed. All the while at the northern sites, which still have a high cover of palsa: 26.3 and 31.6 % at Árbuvuopmi and Vissátvuopmi respectively, show high subsidence rates. This is supported by research showing rapid permafrost degradation in the southernmost palsa complexes in Sweden (Zuidhoff, 2002; Zuidhoff & Kolstrup, 2000) and in the area around and to the south of Tornetrask, since the 1960's (Åkerman & Johansson, 2008; de la Barreda-Bautista et al., 2022; Varner et al., 2022). However, permafrost degradation in palsas have progressed over longer-time periods even in northern Fennoscandia. Here palsas' have decreased in areal extent by 33– 71% over ca. 60 years, with more rapid contraction in recent years in Finmarkvidda, Norway and 54% in Vissátvuopmi, northern most Sweden (Borge et al., 2017; Olvmo et al., 2020) and total loss of palsa complexes has been recorded in the far north eastern parts of Norway (Vorren 2017).

Although there are differences in subsidence rates among sites the region wide permafrost degradation reflects ongoing climatic trends (Fig. 3 and 7). Since 1901 Fennoscandia's climate has become wetter as well as warmer with a greater proportion of the precipitation falling as rain relatively to snow (Hänsel, 2020; Irannezhad et al., 2018; Irannezhad et al., 2017; Vikhamar-Schuler et al., 2016). These trends are reflected in the far north where higher air temperatures, greater precipitation and snow depths has already shifted climatic conditions, in parts of the region, away from those that support permafrost in peatlands e.g. since the 1940's (Åkerman & Johansson, 2008; Borge et al., 2017; Olvmo et al., 2020). Further, deep permafrost boreholes show decadal signals of increasing temperatures in the Scandes mountains suggesting that warmer temperatures have been impacting permafrost since the 1920's (Isaksen et al., 2007). Hence, it seems that climate warming has been impacting permafrost in Fennoscandia for at least 100 years.

As a result of the ongoing trend of increasing permafrost temperatures in palsas in Fennoscandia, their permafrost temperatures are now close to 0°C, making them especially vulnerable to decay in response to further increases in temperatures (Christiansen et al., 2010; Farbrot et al., 2013). Palsa formation is closely linked to the mean annual temperature, with temperatures below -1 to -2°C and limited insulating snow cover over consecutive years needed as a threshold for palsas to form (Vorren, 2017). In this context it is important to note that the MAT in the area was between 0.53 and -1.4°C since 2000 suggesting that at least in parts of the study area the climatic conditions do not support formation of palsa anymore while conditions are marginal for palsa preservation in the entire region.

Although subsidence dominated in the northern sites, uplift was also noted in the study region. Mechanisms that may explain patterns of uplift are formation of new palsa as well as short-lived frost mounds that can form temporarily in the palsa system (Zuidhoff, 2002). Further mechanisms that may result in uplift are changes in the water level of the flooded parts of the peatlands as well as accumulation of plant residues from the

productive fen vegetation parts of the study sites on the peatland surface, reflecting adaptation of the local ecosystem to degraded palsa mounds reflected by changes in remotely sensed terrain surface.

In addition to demonstrating regional permafrost degradation in northern Fennoscandia, this work also provides proof of concept for circumpolar assessments of permafrost degradation using ASPIS InSAR. It enables detection of the areas with rapidly degrading permafrost and deepening active layers but also peat consolidation in areas that have already lost its permafrost (de la Barrada-Bautista *et al.*, 2022). The fact that InSAR data is integrated over  $20\text{m} \times 20\text{m}$  pixels means that the signal of local level degradation may be somewhat dampened (de la Barrada-Bautista *et al.*, 2022). However, the high precision of the change in vertical position means that InSAR is an important tool to employ to detect the initial stages of large-scale permafrost degradation. In concurrence with the literature (Alshammari *et al.*, 2020; Alshammari *et al.*, 2018; Bartsch *et al.*, 2016; de la Barrada-Bautista *et al.*, 2022; Short *et al.*, 2014; van Huissteden *et al.*, 2021), we found the majority (69%) of our results were within the MSE of direction of ground motion change, providing confidence to locate where permafrost is degrading. Currently, the study of long-term trends and drivers using InSAR is somewhat limited by the short collection period of Sentinel 1, but as more data are continued to be collected, methods such as non-linear time series creation will become viable to compare subsidence directly to longer climatic drivers. However, our large-scale assessment of permafrost subsidence provides a baseline to direct, and compare, against future fieldwork monitoring in northern Sweden. As a complement to the ASPIS-InSAR data, the novel roughness thresholding method used here together with contextual data proved a powerful tool to map and monitor changes (Franklin, 2020; König *et al.*, 2019; Otto *et al.*, 2012). This approach could be developed using machine learning methods to model palsa dynamics to better automate the extraction of palsa landform positions (König *et al.*, 2019; Luoto & Seppälä, 2002). If accomplished, the operating extent of this tool could be vastly increased using the Arctic 2m DEM dataset over area where its quality is high enough to allow high resolution mapping of the degrading edges of raised palsa plateaux (Morin, 2016; Karlson *et al.*, 2021). In turn this could be used to remove the stable centre of palsa plateaux and exclusively compare palsa edges to the roughness index, where we would expect to find a stronger correlation than there exists with the current palsa raster cells (Fig. 7a). It has been suggested that small, fragmented, and irregularly shaped palsa are more susceptible to erosion (Borge *et al.*, 2017; Mamet *et al.*, 2017; Beer *et al.* in review). We have not gone as far as to estimate this here but the possible palsa edges inferred from the roughness index, could be built upon for this understanding. Casual analysis of figures 5, 6 and the orthophotos provided in the supplementary materials would support these expectations. Together the ASPIS-InSAR and the DEM derived roughness index metrics offer novel ways of large scale monitoring of permafrost degradation. This will help to quantify the rate of palsa ecosystem collapse and transition to a non-permafrost state.

We conclude that permafrost degradation of palsas is occurring across northern Sweden, with the greatest rates of degradation and largest areas impacted being Sweden's two largest permafrost complexes in the far north. This raises serious concerns that these systems will lose their permafrost entirely in the coming decades especially as climatic conditions are approaching the limits of sustaining palsa (Fewster *et al.*, 2022). The implications of this rapid loss of permafrost is ecosystem collapse and loss, as the permafrost core is fundamental to the existence of palsa. Future research should focus on the implications of this collapse on increased  $\text{CH}_4$  emissions (Glagolev *et al.*, 2011; Turetsky *et al.*, 2020; Varner *et al.*, 2022), carbon loss (Hugelius *et al.*, 2020), and thus the potential for strong climate feedbacks (IPCC, 2021) as well as using longer-time InSAR data as this becomes available to investigate regional variations in climatic drivers of permafrost degradation. Further, our study demonstrates that InSAR together with terrain data can be applied over continuous natural surfaces at a regional-scale to monitor permafrost degradation in palsa, offering a tool for circumpolar monitoring of climate warming impact on these systems.

## 5. Acknowledgement

This work was supported by funding from the University of Nottingham, UK, EU-InterAct funding via the InterAccess programme and the Swedish research council (VR-2021-05767 to M. Siewert). Associated fieldwork was supported by the Climate Impacts Research Centre (CIRC) at Umeå University. Samuel Valman was supported by the EPSRC funded Geospatial Centre for Doctoral Training (EP/S023577/1).



## 6. Author contributions

SV: Carried out the majority of the data analysis and made a significant contribution to data interpretation, writing and finalising the manuscript text. Both SV and MS can be considered to have contributed equally to this work.

MS: Contributed to the conception of the study, contributed DEM and orthophoto data, carried out fieldwork to assess permafrost degradation, contributed and advised on data analysis and interpretation, contributed to structuring, writing, and refining the text. Both MS and SV can be considered to have contributed equally to this work.

DB: Contributed to the conception of the study, advised on the data analysis, and made a significant contribution to finalising the text.

ML: Provided data analysis, support on the InSAR processing, data interpretation, and writing of the text.

DG: Carried out the initial InSAR data processing

BBB: Contributed to the conception of the study and refining the text.

AS: Contributed to the conception of the study and advised on the InSAR data processing

SS: Conceived and directed the study, contributed to data analysis, carried out fieldwork to assess permafrost degradation and made a significant contribution to formulating and finalising the text.

SS, DB, AS and MS secured the funding for the project.

### Code Availability

All the python scripts used to carry out these analyses are available at the github repository:

[https://github.com/SamValman/Permafrost\\_Sweden](https://github.com/SamValman/Permafrost_Sweden).

### Data Availability statement

The Sentinel-1 datasets are freely available and can be obtained by searching and downloading the Interferometric Wide (IW) swath mode products for orbit track numbers 168 and 66 through the Copernicus Open Access Hub (<https://scihub.copernicus.eu/dhus/#/home>). The processed interferometric data and deformation maps are commercially sensitive and may be made available on reasonable request by email addressed to the corresponding author. All other datasets produced during this project will be uploaded on zenodo and the DOI provided once the article has been accepted.

## 522 References

- 523 Åkerman, H. J., & Johansson, M. (2008). Thawing permafrost and thicker active layers in sub-arctic Sweden.  
 524 *Permafrost and Periglacial Processes*, 19(3), 279-292. <https://doi.org/10.1002/ppp.626>
- 525 Alshammari, L., Boyd, D. S., Sowter, A., Marshall, C., Andersen, R., Gilbert, P., Marsh, S., & Large, D. J.  
 526 (2020). Use of Surface Motion Characteristics Determined by InSAR to Assess Peatland Condition  
 527 [<https://doi.org/10.1029/2018JG004953>]. *Journal of Geophysical Research: Biogeosciences*, 125(1),  
 528 e2018JG004953. <https://doi.org/https://doi.org/10.1029/2018JG004953>
- 529 Alshammari, L., Large, D. J., Boyd, D. S., Sowter, A., Anderson, R., Andersen, R., & Marsh, S. (2018). Long-  
 530 Term Peatland Condition Assessment via Surface Motion Monitoring Using the ISBAS DInSAR  
 531 Technique over the Flow Country, Scotland. *Remote Sensing*, 10(7).  
 532 <https://doi.org/10.3390/rs10071103>
- 533 Armstrong McKay, D. I., Staal, A., Abrams, J. F., Winkelmann, R., Sakschewski, B., Loriani, S., Fetzner, I.,  
 534 Cornell, S. E., Rockström, J., & Lenton, T. M. (2022). Exceeding 1.5°C global warming could trigger  
 535 multiple climate tipping points. *Science*, 377(6611), eabn7950.  
 536 <https://doi.org/doi:10.1126/science.abn7950>
- 537 Backe, S. (2014). *Kartering av Sveriges palsmyrar*. Länsstyrelsen.
- 538 Ballantyne C. K. (2018). *Periglacial geomorphology*. John Wiley & Sons.
- 539 Bartsch, A., Widhalm, B., Kuhry, P., Hugelius, G., Palmtag, J., Siewert, M.B., 2016. Can C-band synthetic  
 540 aperture radar be used to estimate soil organic carbon storage in tundra? *Biogeosciences*, 13, 5453-  
 541 5470.
- 542 Beer, J. M., Wang, Y., Way, R., Forget, A. & Colyn, V. 2023. Uncrewed aerial vehicle-based assessments of  
 543 peatland permafrost vulnerability along the Labrador Sea coastline, northern Canada.
- 544 Biskaborn, B. K., Smith, S. L., Noetzi, J., Matthes, H., Vieira, G., Streletskiy, D. A., Schoeneich, P.,  
 545 Romanovsky, V. E., Lewkowicz, A. G., Abramov, A., Allard, M., Boike, J., Cable, W. L.,  
 546 Christiansen, H. H., Delaloye, R., Diekmann, B., Drozdov, D., Etzelmüller, B., Grosse, G., . . . Lantuit,  
 547 H. (2019). Permafrost is warming at a global scale. *Nature Communications*, 10(1), 264.  
 548 <https://doi.org/10.1038/s41467-018-08240-4>
- 549 Borge, A. F., Westermann, S., Solheim, I., & Etzelmüller, B. (2017). Strong degradation of palsas and peat  
 550 plateaus in northern Norway during the last 60 years. *The Cryosphere*, 11(1), 1-16.  
 551 <https://doi.org/10.5194/tc-11-1-2017>
- 552 Bradley, A. V., Andersen, R., Marshall, C., Sowter, A., & Large, D. J. (2022). Identification of typical  
 553 ecohydrological behaviours using InSAR allows landscape-scale mapping of peatland condition. *Earth*  
 554 *Surf. Dynam.*, 10(2), 261-277. <https://doi.org/10.5194/esurf-10-261-2022>
- 555 Chadburn, S. E., Burke, E. J., Cox, P. M., Friedlingstein, P., Hugelius, G., & Westermann, S. (2017). An  
 556 observation-based constraint on permafrost loss as a function of global warming. *Nature Climate*  
 557 *Change*, 7(5), 340-344. <https://doi.org/10.1038/nclimate3262>
- 558 Chen, C.W. and Zebker, H.A., 2001. Two-dimensional phase unwrapping with use of statistical models for cost  
 559 functions in nonlinear optimization. *JOSA A*, 18(2), pp.338-351.
- 560 Christiansen, H. H., Etzelmüller, B., Isaksen, K., Juliussen, H., Farbrøt, H., Humlum, O., Johansson, M.,  
 561 Ingeman-Nielsen, T., Kristensen, L., Hjort, J., Holmlund, P., Sannel, A. B. K., Sigsgaard, C., Åkerman,  
 562 H. J., Foged, N., Blikra, L. H., Pernosky, M. A., & Ødegård, R. S. (2010). The thermal state of  
 563 permafrost in the nordic area during the international polar year 2007–2009. *Permafrost and*  
 564 *Periglacial Processes*, 21(2), 156-181. <https://doi.org/https://doi.org/10.1002/ppp.687>
- 565 Cigna, F., & Sowter, A. (2017). The relationship between intermittent coherence and precision of ISBAS InSAR  
 566 ground motion velocities: ERS-1/2 case studies in the UK. *Remote Sensing of Environment*, 202, 177-  
 567 198. <https://doi.org/https://doi.org/10.1016/j.rse.2017.05.016>
- 568 de la Barreda-Bautista, B., Boyd, D. S., Ledger, M., Siewert, M. B., Chandler, C., Bradley, A. V., Gee, D.,  
 569 Large, D. J., Olofsson, J., Sowter, A., & Sjögersten, S. (2022). Towards a Monitoring Approach for  
 570 Understanding Permafrost Degradation and Linked Subsidence in Arctic Peatlands. *Remote Sensing*,  
 571 14(3). <https://doi.org/10.3390/rs14030444>
- 572 Douglas, T. A., Hiemstra, C. A., Anderson, J. E., Barbato, R. A., Bjella, K. L., Deeb, E. J., Gelvin, A. B.,  
 573 Nelsen, P. E., Newman, S. D., Saari, S. P., & Wagner, A. M. (2021). Recent degradation of interior  
 574 Alaska permafrost mapped with ground surveys, geophysics, deep drilling, and repeat airborne lidar.  
 575 *The Cryosphere*, 15(8), 3555-3575. <https://doi.org/10.5194/tc-15-3555-2021>
- 576 Douglas, T. A., Jorgenson, M. T., Brown, D. R. N., Campbell, S. W., Hiemstra, C. A., Saari, S. P., Bjella, K., &  
 577 Liljedahl, A. K. (2015). Degrading permafrost mapped with electrical resistivity tomography, airborne  
 578 imagery and LiDAR, and seasonal thaw measurements. *GEOPHYSICS*, 81(1), WA71-WA85.  
 579 <https://doi.org/10.1190/geo2015-0149.1>

- ESA (2015). Definition of the TOPS SLC deramping function for products generated by the S-1 IPF. *European Space Agency*. COPE-GSEG-EOPG-TN-14-0025, Issue 1, Revision 2, 22 April 2015.
- Farbrot, H., Isaksen, K., Etzelmüller, B., & Gislén, K. (2013). Ground Thermal Regime and Permafrost Distribution under a Changing Climate in Northern Norway. *Permafrost and Periglacial Processes*, 24(1), 20-38. <https://doi.org/10.1002/ppp.1763>
- Fewster, R. E., Morris, P. J., Ivanovic, R. F., Swindles, G. T., Peregon, A. M., & Smith, C. J. (2022). Imminent loss of climate space for permafrost peatlands in Europe and Western Siberia. *Nature Climate Change*, 12(4), 373-379. <https://doi.org/10.1038/s41558-022-01296-7>
- Franklin, S. E. (2020). Interpretation and use of geomorphometry in remote sensing: a guide and review of integrated applications. *International Journal of Remote Sensing*, 41(19), 7700-7733. <https://doi.org/10.1080/01431161.2020.1792577>
- Fronzek, S., Luoto, M., & Carter, T. (2006). Potential effect of climate change on the distribution of palsa mires in subarctic Fennoscandia. *Climate Research*, 32(1), 1-12. <https://www.int-res.com/abstracts/cr/v32/n1/p1-12/>
- Gee, D., Bateson, L., Sowter, A., Grebby, S., Novellino, A., Cigna, F., Marsh, S., Banton, C., & Wyatt, L. (2017). Ground Motion in Areas of Abandoned Mining: Application of the Intermittent SBAS (ISBAS) to the Northumberland and Durham Coalfield, UK. *Geosciences*, 7(3). <https://doi.org/10.3390/geosciences7030085>
- Gislén, K., Etzelmüller, B., Lüssana, C., Hjort, J., Sannel, A. B. K., Isaksen, K., Westermann, S., Kuhry, P., Christiansen, H. H., Frampton, A., & Åkerman, J. (2017). Permafrost Map for Norway, Sweden and Finland. *Permafrost and Periglacial Processes*, 28(2), 359-378. <https://doi.org/10.1002/ppp.1922>
- Glagolev, M., Kleptsova, I., Filippov, I., Maksyutov, S., & Machida, T. (2011). Regional methane emission from West Siberia mire landscapes. *Environmental Research Letters*, 6(4), 045214.
- Hänsel, S. (2020). Changes in the Characteristics of Dry and Wet Periods in Europe (1851–2015). *Atmosphere*, 11(10), 1080. <https://www.mdpi.com/2073-4433/11/10/1080>
- Harris, C. R., Millman, K. J., van der Walt, S. J., Gommers, R., Virtanen, P., Cournapeau, D., Wieser, E., Taylor, J., Berg, S., Smith, N. J., Kern, R., Picus, M., Hoyer, S., van Kerkwijk, M. H., Brett, M., Haldane, A., del Río, J. F., Wiebe, M., Peterson, P., . . . Oliphant, T. E. (2020). Array programming with NumPy. *Nature*, 585(7825), 357-362. <https://doi.org/10.1038/s41586-020-2649-2>
- Harris, L. I., Richardson, K., Bona, K. A., Davidson, S. J., Finkelstein, S. A., Garneau, M., McLaughlin, J., Nwaishi, F., Olefeldt, D., Packalen, M., Roulet, N. T., Southey, F. M., Strack, M., Webster, K. L., Wilkinson, S. L., & Ray, J. C. (2022). The essential carbon service provided by northern peatlands. *Frontiers in Ecology and the Environment*, 20(4), 222-230. <https://doi.org/10.1002/fee.2437>
- Hugelius, G. A., Loisel, J. A., Chadburn, S. A., Jackson, R. A., Jones, M. A., MacDonald, G., Marushchak, M., Olefeldt, D. A., Packalen, M., Siewert, M. A., Treat, C. A.-O., Turetsky, M., Voigt, C. A., & Yu, Z. A. (2020). Large stocks of peatland carbon and nitrogen are vulnerable to permafrost thaw. *Proceedings of the National Academy of Sciences*, 117(34), 20438-20446. <https://doi.org/10.1073/pnas.1916387117>
- IPCC. (2021). *The Physical Science Basis. Contribution of Working Group I to the Sixth Assessment Report of the Intergovernmental Panel on Climate Change*. Cambridge University Press.
- Irannezhad, M., Moradkhani, H., & Kløve, B. (2018). Spatiotemporal Variability and Trends in Extreme Temperature Events in Finland over the Recent Decades: Influence of Northern Hemisphere Teleconnection Patterns. *Advances in Meteorology*, 2018, 7169840. <https://doi.org/10.1155/2018/7169840>
- Irannezhad, M., Ronkanen, A.-K., Kiani, S., Chen, D., & Kløve, B. (2017). Long-term variability and trends in annual snowfall/total precipitation ratio in Finland and the role of atmospheric circulation patterns. *Cold Regions Science and Technology*, 143, 23-31. <https://doi.org/10.1016/j.coldregions.2017.08.008>
- Isaksen, K., Sollid, J. L., Holmlund, P., & Harris, C. (2007). Recent warming of mountain permafrost in Svalbard and Scandinavia. *Journal of Geophysical Research: Earth Surface*, 112(F2). <https://doi.org/10.1029/2006JF000522>
- Johansson, M., Åkerman, J., Keuper, F., Christensen, T. R., Lantuit, H., & Callaghan, T. V. (2011). Past and Present Permafrost Temperatures in the Abisko Area: Redrilling of Boreholes. *AMBIO*, 40(6), 558. <https://doi.org/10.1007/s13280-011-0163-3>
- Johansson, M., Callaghan, T. V., Bosiö, J., Åkerman, H. J., Jackowicz-Korczynski, M., & Christensen, T. R. (2013). Rapid responses of permafrost and vegetation to experimentally increased snow cover in sub-arctic Sweden. *Environmental Research Letters*, 8(3), 035025. <https://doi.org/10.1088/1748-9326/8/3/035025>

- Karlson, M., bastviken, D. & reese, H. (2021). Error characteristics of pan-arctic digital elevation models and elevation derivatives in northern sweden. *Remote Sensing*, 13, 4653.
- Köchy, M., Hiederer, R., & Freibauer, A. (2015). Global distribution of soil organic carbon – Part 1: Masses and frequency distributions of SOC stocks for the tropics, permafrost regions, wetlands, and the world. *SOIL*, 1(1), 351-365. <https://doi.org/10.5194/soil-1-351-2015>
- König, S., Schultz, J. A., Schoch, A., Blöthe, J., Schrott, L., & Thonfeld, F. (2019). Mountain Permafrost Distribution Modeling—A Geomorphometry-Remote Sensing Approach for the Hohe Tauern National Park, Austria. *Dreiländertagung der DGPF, der OVG und der SGPF in Wien, Österreich—Publikationen der DGPF*, 28.
- Könönen, O. H., Karjalainen, O., Aalto, J., Luoto, M., & Hjort, J. (2022). Environmental spaces for palsas and peat plateaus are disappearing at a circumpolar scale. *The Cryosphere Discuss.*, 2022, 1-37. <https://doi.org/10.5194/tc-2022-135>
- Lantmäteriet. (2021). Orthophoto (Ortofoto) [Online]. Version 2.7. Available at: [https://www.lantmateriet.se/globalassets/geodata/geodataprodukter/flyg--och-satellitbilder/e\\_pb\\_ortofoto.pdf](https://www.lantmateriet.se/globalassets/geodata/geodataprodukter/flyg--och-satellitbilder/e_pb_ortofoto.pdf). Accessed on 10<sup>th</sup> January 2024.
- Liu, L., Zhang, T., & Wahr, J. (2010). InSAR measurements of surface deformation over permafrost on the North Slope of Alaska. *Journal of Geophysical Research: Earth Surface*, 115(F3). <https://doi.org/10.1029/2009JF001547>
- Luoto, M., & Seppälä, M. (2002). Modelling the distribution of palsas in Finnish Lapland with logistic regression and GIS. *Permafrost and Periglacial Processes*, 13(1), 17-28.
- Luoto, M., & Seppälä, M. (2003). Thermokarst ponds as indicators of the former distribution of palsas in Finnish Lapland. *Permafrost and Periglacial Processes*, 14(1), 19-27. <https://doi.org/10.1002/ppp.441>
- Mamet, S. D., Chun, K. P., Kershaw, G. G. L., Loranty, M. M., & Kershaw, G. P. (2017). Recent Increases in Permafrost Thaw Rates and Areal Loss of Palsas in the Western Northwest Territories, Canada. *Permafrost and Periglacial Processes*, 28, 619-633. <https://doi.org/10.1002/ppp.1951>
- Markkula, I., Turunen, M., & Rasmus, S. (2019). A review of climate change impacts on the ecosystem services in the Saami Homeland in Finland. *Science of The Total Environment*, 692, 1070-1085. <https://doi.org/https://doi.org/10.1016/j.scitotenv.2019.07.272>
- Matthews, J. A., Dahl, S.-O., Berrisford, M. S., & Nesje, A. (1997). Cyclic Development and Thermokarstic Degradation of Palsas in the Mid-Alpine Zone at Leirpullan, Dovrefjell, Southern Norway. *Permafrost and Periglacial Processes*, 8(1), 107-122. [https://doi.org/https://doi.org/10.1002/\(SICI\)1099-1530\(199701\)8:1<107::AID-PPP237>3.0.CO;2-Z](https://doi.org/https://doi.org/10.1002/(SICI)1099-1530(199701)8:1<107::AID-PPP237>3.0.CO;2-Z)
- McKinney, W. (2011). pandas: a Foundational Python Library for Data Analysis and Statistics.
- Miglovets, M., Zagirova, S., Goncharova, N., & Mikhailov, O. (2021). Methane Emission from Palsa Mires in Northeastern European Russia. *Russian Meteorology and Hydrology*, 46(1), 52-59. <https://doi.org/10.3103/S1068373921010076>
- Morin, P., Porter, C., Cloutier, M., Howat, I., Noh, M.J., Willis, M., Bates, B., Williamson, C. and Peterman, K. (2016). ArcticDEM; a publically available, high resolution elevation model of the Arctic. EGU General Assembly 2016, Vienna, Austria.
- Obu, J. (2021). How Much of the Earth's Surface is Underlain by Permafrost? *Journal of Geophysical Research: Earth Surface*, 126(5), e2021JF006123. <https://doi.org/https://doi.org/10.1029/2021JF006123>
- Obu, J., Westermann, S., Kääb, A., & Bartsch, A. (2018). Ground Temperature Map, 2000-2016, Northern Hemisphere Permafrost PANGAEA. <https://doi.org/10.1594/PANGAEA.888600>
- Olvmo, M., Holmer, B., Thorsson, S., Reese, H., & Lindberg, F. (2020). Sub-arctic palsa degradation and the role of climatic drivers in the largest coherent palsa mire complex in Sweden (Vissátvuopmi), 1955–2016. *Scientific Reports*, 10(1), 8937. <https://doi.org/10.1038/s41598-020-65719-1>
- Otto, J. c., Keuschnig, M., Götz, J., Marbach, M., & Schrott, L. (2012). Detection of mountain permafrost by combining high resolution surface and subsurface information—an example from the Glatzbach catchment, Austrian Alps. *Geografiska Annaler: Series A, Physical Geography*, 94(1), 43-57. <https://doi.org/10.1111/j.1468-0459.2012.00455.x>
- QGIS, D. (2022). QGIS User Guide: 24.2.1 Raster Analysis. Retrieved from [https://docs.qgis.org/3.16/en/docs/user\\_manual/processing\\_algs/gdal/rasteranalysis.html#hillshade](https://docs.qgis.org/3.16/en/docs/user_manual/processing_algs/gdal/rasteranalysis.html#hillshade)
- Ramage, J., Jungsberg, L., Wang, S. N., Westermann, S., Lantuit, H., & Heleniak, T. (2021). Population living on permafrost in the Arctic. *Population and Environment*, 43(1), 22-38. <https://doi.org/10.1007/s11111-020-00370-6>
- Reinosch, E., Buckel, J., Dong, J., Gerke, M., Baade, J., & Riedel, B. (2020). InSAR time series analysis of seasonal surface displacement dynamics on the Tibetan Plateau. *The Cryosphere*, 14(5), 1633-1650. <https://doi.org/10.5194/tc-14-1633-2020>
- Sannel, A. B. K. (2020). Ground temperature and snow depth variability within a subarctic peat plateau landscape. *Permafrost and Periglacial Processes*, 31(2), 255-263. <https://doi.org/10.1002/ppp.2045>



699 Sannel, A. B. K., Hugelius, G., Jansson, P., & Kuhry, P. (2016). Permafrost Warming in a Subarctic Peatland –  
700 Which Meteorological Controls are Most Important?. *Permafrost and Periglacial Processes*, 27(2),  
701 177-188. <https://doi.org/10.1002/ppp.1862>

702 Sannel, A. B. K., & Kuhry, P. (2011). Warming-induced destabilization of peat plateau/thermokarst lake  
703 complexes. *Journal of Geophysical Research: Biogeosciences*, 116(G3).  
704 <https://doi.org/10.1029/2010JG001635>

705 Schuur, E. A. G., McGuire, A. D., Schädel, C., Grosse, G., Harden, J. W., Hayes, D. J., Hugelius, G., Koven, C.  
706 D., Kuhry, P., Lawrence, D. M., Natali, S. M., Olefeldt, D., Romanovsky, V. E., Schaefer, K.,  
707 Turetsky, M. R., Treat, C. C., & Vonk, J. E. (2015). Climate change and the permafrost carbon  
708 feedback. *Nature*, 520(7546), 171-179. <https://doi.org/10.1038/nature14338>

709 Schuur, E. A. G., Vogel, J. G., Crummer, K. G., Lee, H., Sickman, J. O., & Osterkamp, T. E. (2009). The effect  
710 of permafrost thaw on old carbon release and net carbon exchange from tundra. *Nature*, 459(7246),  
711 556-559. <https://doi.org/10.1038/nature08031>

712 Seppälä, M. (2011). Synthesis of studies of palsa formation underlining the importance of local environmental  
713 and physical characteristics. *Quaternary Research*, 75(2), 366-370.  
714 <https://doi.org/10.1016/j.yqres.2010.09.007>

715 Siewert, M.B., 2018. High-resolution digital mapping of soil organic carbon in permafrost terrain using machine  
716 learning: a case study in a sub-Arctic peatland environment. *Biogeosciences*, 15, 1663-1682.

717 Sjöberg, Y., Siewert, M.B., Rudy, A.C.A., Paquette, M., Bouchard, F., Malenfant-Lepage, J., Fritz, M., 2020.  
718 Hot trends and impact in permafrost science. *Permafrost and Periglacial Processes*, 31, 461-471.

719 Short, N., LeBlanc, A.-M., Sladen, W., Oldenborger, G., Mathon-Dufour, V., & Brisco, B. (2014).  
720 RADARSAT-2 D-InSAR for ground displacement in permafrost terrain, validation from Iqaluit  
721 Airport, Baffin Island, Canada. *Remote Sensing of Environment*, 141, 40-51.  
722 <https://doi.org/https://doi.org/10.1016/j.rse.2013.10.016>

723 SMHI, (2022). Download Meteorological observations. Retrieved from  
724 [https://www.smhi.se/data/meteorologi/ladda-ner-meteorologiska-](https://www.smhi.se/data/meteorologi/ladda-ner-meteorologiska-observationer#param=airtemperatureInstant,stations=core,stationid=191910)  
725 [observationer#param=airtemperatureInstant,stations=core,stationid=191910](https://www.smhi.se/data/meteorologi/ladda-ner-meteorologiska-observationer#param=airtemperatureInstant,stations=core,stationid=191910)

726 Smith, M. W., & Riseborough, D. W. (1996). Permafrost monitoring and detection of climate change.  
727 *Permafrost and Periglacial Processes*, 7(4), 301-309.  
728 [https://doi.org/https://doi.org/10.1002/\(SICI\)1099-1530\(199610\)7:4<301::AID-PPP231>3.0.CO;2-R](https://doi.org/https://doi.org/10.1002/(SICI)1099-1530(199610)7:4<301::AID-PPP231>3.0.CO;2-R)

729 Smith, S.L, O'Neill, H.B., Isaksen, K., Noetzli, J. and Romanovsky, V.E. (2022). The changing thermal state of  
730 permafrost. *Nature Reviews Earth and Environment*, 3, 10-23.

731 Sowter, A., Bin Che Amat, M., Cigna, F., Marsh, S., Athab, A., & Alshammari, L. (2016). Mexico City land  
732 subsidence in 2014–2015 with Sentinel-1 IW TOPS: Results using the Intermittent SBAS (ISBAS)  
733 technique. *International Journal of Applied Earth Observation and Geoinformation*, 52, 230-242.  
734 <https://doi.org/https://doi.org/10.1016/j.jag.2016.06.015>

735 Spyder Website Contributors. (2021). Spyder IDE. Retrieved from <https://www.spyder-ide.org/>

736 Swingedouw, D., Ifejika Speranza, C., Bartsch, A., Durand, G., Jamet, C., Beaugrand, G., & Conversi, A.  
737 (2020). Early Warning from Space for a Few Key Tipping Points in Physical, Biological, and Social-  
738 Ecological Systems. *Surveys in Geophysics*, 41(6), 1237-1284. [https://doi.org/10.1007/s10712-020-](https://doi.org/10.1007/s10712-020-09604-6)  
739 [09604-6](https://doi.org/10.1007/s10712-020-09604-6)

740 Tarnocai, C., Canadell, J. G., Schuur, E. A. G., Kuhry, P., Mazhitova, G., & Zimov, S. (2009). Soil organic  
741 carbon pools in the northern circumpolar permafrost region. *Global Biogeochemical Cycles*, 23(2).  
742 <https://doi.org/https://doi.org/10.1029/2008GB003327>

743 Torres, R., Snoeijs, P., Geudtner, D., Bibby, D., Davidson, M., Attema, E., Potin, P., Rommen, B., Floury, N.,  
744 Brown, M., Traver, I. N., Deghaye, P., Duesmann, B., Rosich, B., Miranda, N., Bruno, C., L'Abbate,  
745 M., Croci, R., Pietropaolo, A., . . . Rostan, F. (2012). GMES Sentinel-1 mission. *Remote Sensing of*  
746 *Environment*, 120, 9-24. <https://doi.org/https://doi.org/10.1016/j.rse.2011.05.028>

747 Turetsky, M. R., Abbott, B. W., Jones, M. C., Anthony, K. W., Olefeldt, D., Schuur, E. A. G., Grosse, G.,  
748 Kuhry, P., Hugelius, G., Koven, C., Lawrence, D. M., Gibson, C., Sannel, A. B. K., & McGuire, A. D.  
749 (2020). Carbon release through abrupt permafrost thaw. *Nature Geoscience*, 13(2), 138-143.  
750 <https://doi.org/10.1038/s41561-019-0526-0>

751 Vallée, S., & Payette, S. (2007). Collapse of permafrost mounds along a subarctic river over the last 100 years  
752 (northern Québec). *Geomorphology*, 90, 162-170. <https://doi.org/10.1016/j.geomorph.2007.01.019>

753 van Huissteden, J., Teshebaeva, K., Cheung, Y., Magnússon, R. Í., Noorbergen, H., Karsanaev, S. V., Maximov,  
754 T. C., & Dolman, A. J. (2021). Geomorphology and InSAR-Tracked Surface Displacements in an Ice-  
755 Rich Yedoma Landscape. *Frontiers in Earth Science*, 9(724).  
756 <https://doi.org/10.3389/feart.2021.680565>

757 Varner, R. K., Crill, P. M., Frohling, S., McCalley, C. K., Burke, S. A., Chanton, J. P., Holmes, M. E., null, n.,  
758 Saleska, S., & Palace, M. W. (2022). Permafrost thaw driven changes in hydrology and vegetation

- cover increase trace gas emissions and climate forcing in Stordalen Mire from 1970 to 2014. *Philosophical Transactions of the Royal Society A: Mathematical, Physical and Engineering Sciences*, 380(2215), 20210022. <https://doi.org/10.1098/rsta.2021.0022>
- Vikhamar-Schuler, D., Isaksen, K., Haugen, J. E., Tømmervik, H., Luks, B., Schuler, T. V., & Bjerke, J. W. (2016). Changes in Winter Warming Events in the Nordic Arctic Region. *Journal of Climate*, 29(17), 6223-6244. <https://doi.org/10.1175/JCLI-D-15-0763.1>
- Virtanen, P., Gommers, R., Oliphant, T. E., Haberland, M., Reddy, T., Cournapeau, D., Burovski, E., Peterson, P., Weckesser, W., & Bright, J. (2020). SciPy 1.0: fundamental algorithms for scientific computing in Python. *Nature methods*, 17(3), 261-272.
- Vorren, K.-D. (2017). The first permafrost cycle in Færdesmyra, eastern Finnmark, Norway? *Norsk Geografisk Tidsskrift - Norwegian Journal of Geography*, 71(2), 114-121. <https://doi.org/10.1080/00291951.2017.1316309>
- Zuidhoff, F. S. (2002). Recent decay of a single palsa in relation to weather conditions between 1996 and 2000 in Laivadalén, northern Sweden. *Geografiska Annaler Series A-Physical Geography*, 84A(2), 103-111. <https://doi.org/10.1111/j.0435-3676.2002.00164.x>
- Zuidhoff, F. S., & Kolstrup, E. (2000). Changes in palsa distribution in relation to climate change in Laivadalén, northern Sweden, especially 1960–1997. *Permafrost and Periglacial Processes*, 11(1), 55-69. [https://doi.org/https://doi.org/10.1002/\(SICI\)1099-1530\(200001/03\)11:1](https://doi.org/https://doi.org/10.1002/(SICI)1099-1530(200001/03)11:1)